Geophysical Research Letters

RESEARCH LETTER
10.1029/2023GL103885

Self-Reversed Magnetization in Sediments Caused by Greigite Alteration

Liao Chang[1,2], Zhaowen Pei[1], Pengfei Xue[1], Shishun Wang[1,3], Zhaoping Wang[1], Wout Krijgsman[4], and Mark J. Dekkers[4]

[1]Laboratory of Orogenic Belts and Crustal Evolution, School of Earth and Space Sciences, Peking University, Beijing, China, [2]Laboratory for Marine Geology, Qingdao National Laboratory for Marine Science and Technology, Qingdao, China, [3]Now at Key Laboratory of Submarine Geosciences, Second Institute of Oceanography, Ministry of Natural Resources, Hangzhou, China, [4]Paleomagnetic Laboratory Fort Hoofddijk, Department of Earth Sciences, Utrecht University, Utrecht, The Netherlands

Key Points:

- Surface alteration of diagenetic greigite to magnetite and pyrrhotite causes magnetic softening and multipolarity remanence
- The original microtextures are preserved during iron sulfide alteration and the alteration extent is size-dependent
- A new multi-phase self-reversal model of diagenetic greigite is proposed that has broad geochronological and geophysical implications

Supporting Information:

Supporting Information may be found in the online version of this article.

Correspondence to:

L. Chang,
liao.chang@pku.edu.cn

Citation:

Chang, L., Pei, Z., Xue, P., Wang, S., Wang, Z., Krijgsman, W., & Dekkers, M. J. (2023). Self-reversed magnetization in sediments caused by greigite alteration. *Geophysical Research Letters*, *50*, e2023GL103885. https://doi.org/10.1029/2023GL103885

Received 28 MAR 2023
Accepted 13 JUN 2023

Author Contributions:

Conceptualization: Liao Chang, Wout Krijgsman, Mark J. Dekkers
Data curation: Liao Chang
Formal analysis: Liao Chang, Zhaowen Pei, Pengfei Xue, Shishun Wang, Zhaoping Wang, Wout Krijgsman
Funding acquisition: Liao Chang
Investigation: Liao Chang, Zhaowen Pei, Pengfei Xue, Shishun Wang, Zhaoping Wang
Methodology: Liao Chang
Project Administration: Liao Chang
Resources: Liao Chang
Supervision: Liao Chang
Validation: Liao Chang

Abstract

Multipolarity remanence in greigite-bearing sediments has long been recognized, but the cause of this anomalous remanence behavior is not well understood. Here, we use electron microscopic and magnetic analyses to investigate the origin of such multipolarity in Miocene greigite-bearing sediments from the Pannonian Basin (Hungary). We find a magnetic softening and partial transformation of iron sulfides to magnetite and pyrrhotite from "single-polarity" to "multi-polarity" samples. The inward alteration of sulfide grains is topotactic and is size-dependent with higher alteration in smaller grains. We propose a multi-phase self-reversal chemical remanent magnetization (CRM) mechanism in altered greigite: the neoformed magnetite/pyrrhotite shell acquires a CRM coupled in the opposite direction to the primary CRM of the greigite core, likely through magnetostatic interactions or interfacial exchange interactions between the closely contacting core and shell. This new greigite self-reversal model can explain the commonly observed antiparallel polarities and has broad geochronological, tectonic and paleoenvironmental implications.

Plain Language Summary

Some magnetic minerals in nature can be magnetized opposite to the external geomagnetic and planetary magnetic fields—a peculiar phenomenon called "self-reversal." A self-reversal magnetization process is typically observed to occur in igneous rocks during cooling in an external field. Here, using magnetic and microscopic analyses we demonstrate that sediments containing authigenic ferrimagnetic iron sulfide mineral—greigite—can acquire a self-reversed magnetization during progressive surface alteration of greigite nanoparticles. Surface alteration produces new "magnetic shells" that are magnetized opposite to the magnetization of the parent greigite core through magnetic interactions due to the close contact between the core and shell. Post-depositional sedimentary processes, for example, percolation of fluids or oxygenation could trigger surface alteration that leads to "self-reversal" and complicate the primary magnetization records. This self-reversal mechanism can explain the commonly reported anomalous magnetization records of authigenic greigite; it is very useful for correct interpretations of tectonic and paleoenvironmental processes, and geological age frames of iron sulfide bearing sediment sequences.

1. Introduction

Greigite (Fe_3S_4) is an inverse iron thiospinel with a ferrimagnetic structure similar to that of magnetite (Fe_3O_4) (Chang et al., 2008; Chang, Rainford, et al., 2009; Skinner et al., 1964). Greigite is common in natural environments and occurs in two main modes: (a) formed inorganically through microbially mediated sulfate-reduction, referred to as "diagenetic greigite" (e.g., Berner, 1984; Rowan & Roberts, 2006); and (b) formed biogenically by intracellular biomineralization in sulfidic magnetotactic bacteria, referred to as "biogenic greigite" (Farina et al., 1990; Mann et al., 1990). Diagenetic greigite has been widely identified and carries important paleomagnetic and environmental information (see Roberts et al., 2011 and references therein). Fossilized biogenic greigite in sediments can be used as a reliable paleomagnetic recorder and paleoenvironmental proxy in anoxic environments (Chang et al., 2014; Reinholdsson et al., 2013; Vasiliev et al., 2008).

Interpreting paleomagnetic records carried by greigite can be problematic: greigite can grow authigenically any time after sediment formation, as long as suitable bio-geochemical conditions prevail leading to partial or fully remagnetized strata (Roberts & Weaver, 2005; Sagnotti et al., 2005). In some cases it is difficult to distinguish late diagenetic greigite growth from quasi-syn-sedimentary greigite formation (Rowan & Roberts, 2005). Anomalous

Visualization: Liao Chang, Zhaowen Pei, Pengfei Xue, Shishun Wang
Writing – original draft: Liao Chang
Writing – review & editing: Zhaowen Pei, Pengfei Xue, Shishun Wang, Zhaoping Wang, Wout Krijgsman, Mark J. Dekkers

multipolarity magnetization is often seen in published thermal demagnetization data for greigite-bearing sediments (e.g., Florindo & Sagnotti, 1995; Horng et al., 1998; Liu et al., 2014; Rowan & Roberts, 2005, 2006; Turner, 2001), but the cause of this anomalous paleomagnetic behavior is not well understood. Multiple mechanisms have been proposed, including remagnetization due to late diagenetic greigite growth (e.g., Rowan & Roberts, 2005, 2006), magnetic mineral mixtures (e.g., Turner, 2001), and possible self-reversal (Florindo & Sagnotti, 1995; Horng et al., 1998). Each mechanism would imply a different cause and timing of natural remanent magnetization (NRM) acquisition that hinders correct interpretations of magnetostratigraphic and environmental records of greigite-bearing sediments.

Recently, anomalous paleomagnetic signals were observed in drill cores from the Pannonian Basin (Hungary); they were interpreted to be due to a mixture of framboidal greigite and greigite in silicates with different timing (Kelder et al., 2018). Here, we perform combined paleomagnetic, rock magnetic, and electron microscopic analyses to investigate the origin of the multipolarity remanence in these greigite-bearing sediments. The link between NRM behavior, rock magnetic properties, and microscopic magnetic mineral populations is unveiled, resulting in a new model of NRM acquisition that can explain the anomalous magnetization commonly observed in greigite-bearing sediments.

2. Samples and Methods

Greigite-bearing gray mudstones were sampled from the drill core PAET-34 in the Pannonian Basin (Hungary) following standard paleomagnetic procedures (Kelder et al., 2018; Magyar et al., 2019). Fourteen samples with distinct stepwise thermal demagnetization behavior were scrutinized. Remanence after thermal and alternating field (AF) demagnetization was measured on a 2G Enterprises cryogenic magnetometer at Utrecht University (The Netherlands), and at Peking University (PKU, Beijing), respectively. Hysteresis loops, first-order reversal curve (FORC) diagrams (Roberts et al., 2000), isothermal remanent magnetization (IRM) acquisition and backfield demagnetization curves, and low-temperature magnetic properties were measured, using a Princeton MicroMag 3900 vibrating sample magnetometer at the Research School of Earth Sciences, the Australian National University (Canberra), and a Quantum Design magnetic property measurement system (model MPMS3) at the School of Physics, PKU. IRM acquisition and backfield curves were measured in 80 logarithmically spaced steps up to 1 T. FORC settings of 500 mT saturation field, 200 ms averaging time, ±60 mT B_u, 150 mT B_c, and 150 FORCs were used. Classic low-temperature cycling (LTC) of a room-temperature saturation IRM (SIRM), and SIRM warming curves after field-cooling (FC) treatment in a 2.5-Tesla field were measured with a 2-K/min rate. Magnetic susceptibility κ was measured using an AGICO Kappabridge (model MFK-1FA) at PKU.

Rock thin sections were imaged with a FEI QUANTA-650FEG field-emission (FE) scanning electron microscope (SEM). Energy dispersive spectra (EDS) were measured as single points and maps. Transmission electron microscope (TEM) thin-film samples were prepared in situ on rock thin sections using a FEI Helios G4 focused ion beam (FIB) system operating at 30 kV. Bright-field TEM imaging, lattice fringes, selected-area electron diffraction (SAED), and EDS analyses were performed to quantify microtextures and mineral phases with a FEI Tecnai F20 FE-TEM operating at 200 kV. All microscopic analyses were made at PKU.

3. Paleomagnetic and Rock Magnetic Data

Three main groups of thermal demagnetization behavior can be distinguished according to the nature of antiparallel remanence components (Kelder et al., 2018): "single-polarity" (S-type), "multi-polarity" (M-type), and "transitional-polarity" (T-type) (Figure 1a–1c; Figures S1a–S1c in Supporting Information S1). The S-type samples have one major characteristic remanent magnetization (ChRM) component demagnetized between ~100° and 420°C and a minor viscous remanent magnetization (VRM) overprint demagnetized below ~100°C (Figure 1a). The M-type samples have composite multipolarities with antiparallel NRM components (Figure 1c): low-temperature, medium-temperature, and high-temperature components with characteristic demagnetization ranges of ~100° to 230°–250°C, 230°–250° to 300°–310°C, and 300°–310° to 350°C, respectively. The T-type samples have demagnetization behavior between the S- and M-type samples: they exhibit the antiparallel components of remanence, but the antiparallel component is much smaller than that in the M-type samples and the demagnetization track does not cross quadrants in the vector component diagrams (Figure 1b). Most samples show a nearly complete demagnetization at 420°C. Only some S-type samples have a minor contribution from

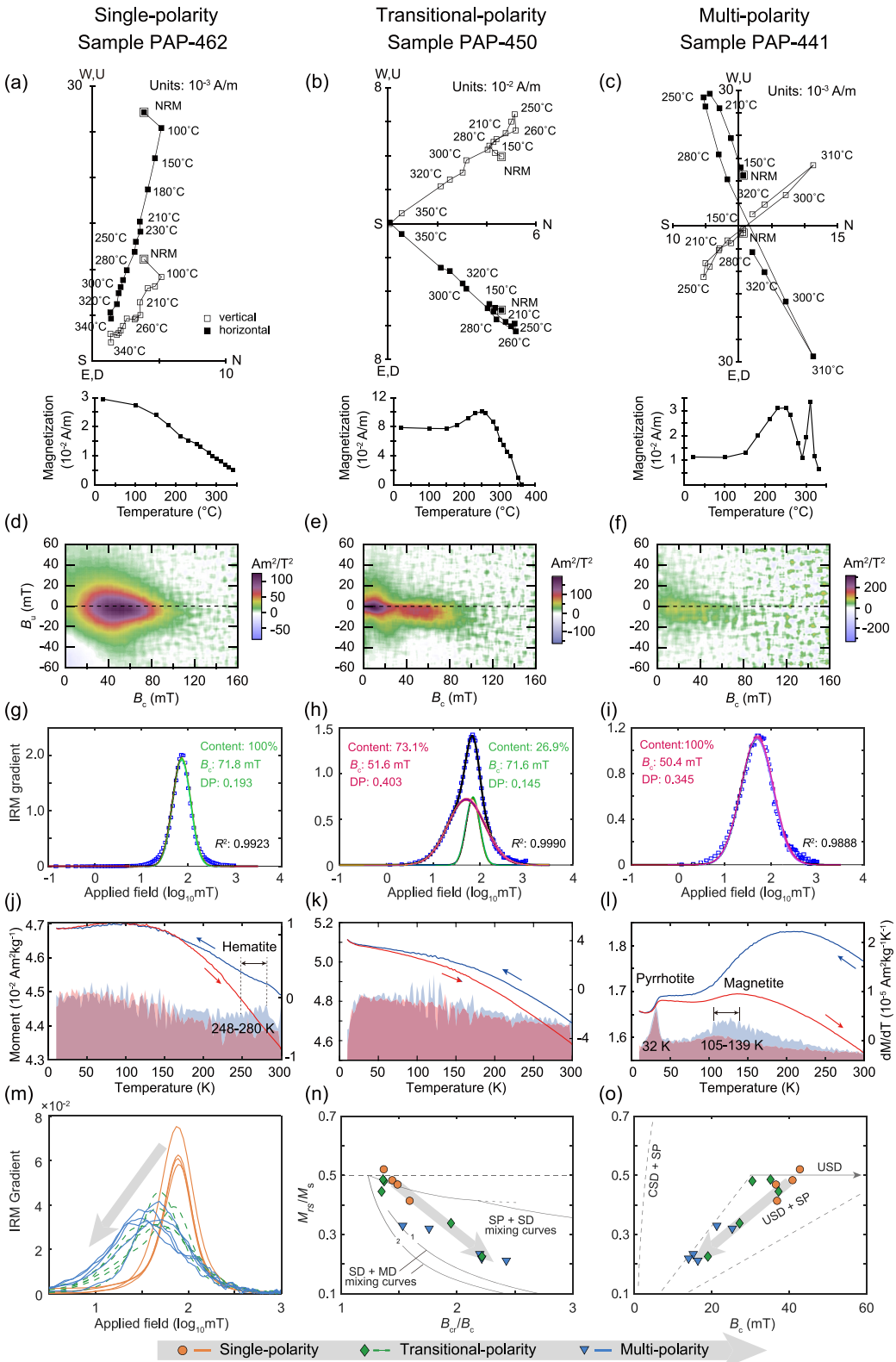

Figure 1.

higher temperature remanence component (~500°–580°C) to the NRM (Kelder et al., 2018). AF demagnetization of an S-type sample (Figure S2a in Supporting Information S1) indicates gyroremanent magnetization (GRM) with increasing remanence at ~60–80 mT AF field commonly observed in diagenetic greigite (Fu et al., 2008; Snowball, 1997). It was recognized by Kelder et al. (2018) that the multipolarity components cannot be resolved by AF demagnetization because of significant coercivity overlap (Figure S2 in Supporting Information S1).

The S-type samples have high B_c (~37–43 mT), high B_{cr} (~54–59 mT), high M_{rs}/M_s (~0.41–0.52), and high SIRM/κ values (~36–141 × 10^3 A/m; Table S1 in Supporting Information S1), and FORC diagrams of high-coercivity concentric contours (B_c peaks at ~40–60 mT) with a large vertical spread (Figure 1d). Their major IRM component has median acquisition coercivity ($B_{1/2}$) values of ~70–80 mT and narrow dispersion parameters (DP) of ~0.16–0.19 (Figure 1g; Figures S1, S3, Table S2 in Supporting Information S1). Those features are typical of strongly interacting single-domain (SD) assemblages reported for diagenetic greigite (Chang et al., 2014; Roberts et al., 2000, 2011; Vasiliev et al., 2008). Compared to the S-type samples, the M-type samples have lower B_c (~14–25 mT), M_{rs}/M_s (~0.21–0.32), and SIRM/κ values (~7–13 × 10^3 A/m; Tables S1, S2 in Supporting Information S1), FORC diagrams of low-coercivity (peak of ~10–20 mT) interacting assemblages (Figure 1f), and a major IRM component with decreased coercivity ($B_{1/2}$ of ~40–53 mT) and distinctly larger DP values of ~0.30–0.44 (Figure 1i; Figures S1, S3, Table S2 in Supporting Information S1). Rock magnetic properties for the T-type samples (Figures 1e and 1h; Figures S1 and S3 in Supporting Information S1) show a mixture of the S-type and M-type samples: FORC diagrams contain a low-coercivity and a high-coercivity components (Figure 1e); IRM gradient curves are fitted with a broader low-coercivity component overlapped with a narrower high-coercivity component (Figure 1h). Some T-type samples show complex mixture behavior and have medium coercivity values between the S- and M-type samples (Figures S1 and S3, Tables S1 and S2 in Supporting Information S1). Magnetic properties for the studied samples here are also different from those of typical biogenic greigite which have a central-ridge FORC signature (Bai, Chang, Pei, et al., 2022; Chang et al., 2014; Chen et al., 2014; Reinholdsson et al., 2013).

Low-temperature magnetic measurements were performed to investigate the magnetic minerology for the three sample types based on characteristic low-temperature phase transitions. The presence of stoichiometric magnetite in the S-type samples can be ruled out because of the absence of the Verwey transition (T_V) (Figure 1j; Figures S1j and S4a in Supporting Information S1), which is consistent with the dominant presence of greigite without any known low-temperature transition (Chang, Roberts, et al., 2009). Low-temperature data for some S-type samples show the Morin (1950) transition in hematite (α-Fe_2O_3) (Figure 1j). LTC curves and SIRM warming curves for the M-type and T-type samples indicate a phase transition temperature of ~30–32 K (Figure 1l, Figure S4 in Supporting Information S1) associated with monoclinic pyrrhotite (Fe_7S_8) (Rochette et al., 1990) and a broad T_V (Figure 1l) in partially oxidized magnetite (Özdemir et al., 1993).

Plots of IRM gradient curves (Figure 1m), hysteresis loops (Figure S5a in Supporting Information S1), the SIRM/κ-B_{cr} plot (Figure S5b in Supporting Information S1), the Day plot (Day et al., 1977), and the Néel (1955) diagram (Figures 1n and 1o) indicate a magnetic softening trend from the S-type to the T- and M-type samples: data move from the high-coercivity interacting SD region to the low-coercivity region with more superparamagnetic (SP) and/or vortex grains.

4. Electron Microscopic Observations and Possible Reaction Pathways of Greigite Alteration

SEM observations reveal abundant authigenic greigite and pyrite (FeS_2) in all studied samples (Figure 2) with characteristic microtextures of framboids, euhedral crystals, and greigite grown in silicate cleavages (e.g., Kelder et al., 2018; Roberts & Weaver, 2005; Rowan & Roberts, 2005, 2006). The sulfide grains of the S-type and

Figure 1. (a–l) Paleomagnetic and rock magnetic results of representative samples with "single-polarity" (S-type), "transitional-polarity" (T-type), and "multi-polarity" (M-type) behavior, and (m–o) trend of hysteresis properties. (a–c) Vector component diagrams with the corresponding remanence decay curve during stepwise thermal demagnetization produced using the software PuffinPlot (Lurcock & Wilson, 2012). Temperatures of most thermal demagnetization steps are indicated on the vector component diagrams. (d–f) FORC diagrams processed using the FORCinel version 3.06 (Harrison & Feinberg, 2008) with a smoothing factor (Roberts et al., 2000) of 6. (g–i) Unmixed IRM gradient curves following the procedure of Kruiver et al. (2001) using the software BatchUnMix (Bai, Chang, Xue, & Wang, 2022). (j–l) Low-temperature cycling curves of a saturation remanence. The cooling and warming curves are indicated by blue and red arrows, respectively. Derivatives are shown in the background with the low-temperature phase transition temperatures of constituent magnetic minerals marked. (m) The first derivatives of isothermal remanent magnetization acquisition curves. (n) Day plot (Day et al., 1977) with Dunlop (2002) mixing lines for reference. (o) Néel (1955) plot with micromagnetic interpretations for magnetite calculated by Tauxe et al. (2002) for reference. SP = superparamagnetic, SD = single domain, MD = multidomain, CSD = cubic single domain, USD = uniaxial single domain. Gray arrows in (m–o) indicate data trends with increasing alteration.

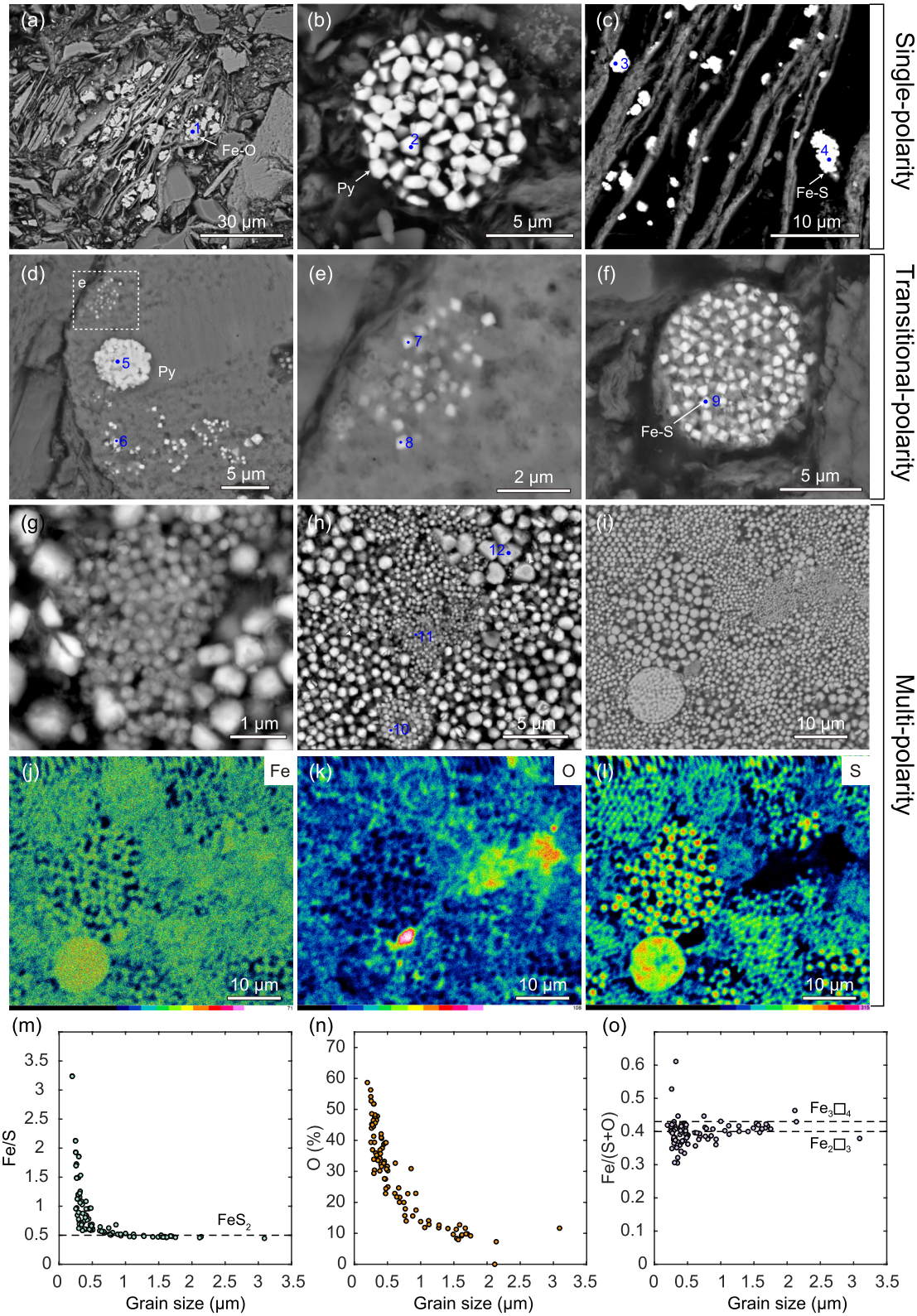

Figure 2.

M-type samples appear to show distinct oxidation levels: the S-type samples contain nearly stoichiometric greigite and pyrite (Figures 2a–2c), whereas the iron sulfide crystals (bright particles in Figures 2d–2i) in the M-type and T-type samples were altered or partially altered to iron oxides (gray particles in Figures 2d–2i). The oxidation degree appears visually to be grain-size dependent, where very fine grains were converted completely to iron oxides and larger particles typically have oxidation shells (Figures 2d–2l). This grain size-dependent oxidation is confirmed by EDS mapping (Figures 2j–2l) and EDS point analysis (Figure S6 in Supporting Information S1) on a large number of crystals in the M-type samples (Figures 2m–2o). It can be explained by a tendency for fine particles to be affected more by alteration due to their larger surface area to volume ratios.

TEM observations on a FIB milling sample with M-type behavior (sample "PAP 441") reveal grain clusters with variable sizes (Figures 3a–3e). EDS mapping indicates the common occurrence of core-shell structure with oxygen-enriched shells surrounding iron sulfide grain cores (Figures 3g, 3k, and 3s), suggesting pervasive alteration of iron sulfides. High-resolution TEM imaging and SAED patterns of the altered iron sulfide grains suggest complex crystalline materials (Figures 3m–3q). The mineral phases in the altered shells can be confidently determined to be pyrrhotite (yellow in Figures 3m and 3n) and magnetite (red in Figure 3p) from a combination of electron diffraction and EDS analysis (Figure 3). The randomly distributed lattice fringes (Figures 3m and 3p) and ring-like diffraction patterns (Figure 3n) indicate that the pyrrhotite and magnetite shells are typically polycrystalline. For larger iron sulfide grains (Figure S7 in Supporting Information S1), lattice fringes and diffraction patterns typically show a crystal structure of pyrite (blue in Figures S7b, S7c in Supporting Information S1), mostly with surficial alteration (Figures S8g, S8k in Supporting Information S1).

Possible reaction pathways for magnetite formation involve (e.g., Wang & Chang, 2022):

$$Fe^{2+} + 2\,OH^- \rightarrow Fe(OH)_2 \quad (1)$$

$$Fe^{3+} + 3\,OH^- \rightarrow Fe(OH)_3 \quad (2)$$

$$Fe(OH)_3 \rightarrow \alpha FeOOH + H_2O \quad (3)$$

$$Fe(OH)_2 + 2\,\alpha FeOOH \rightarrow Fe_3O_4 + 2\,H_2O \quad (4)$$

A possible transformation reaction of greigite into pyrrhotite can be described:

$$7\,Fe_3S_4 \rightarrow 3\,Fe_7S_8 + 4\,S^0 \quad (5)$$

The inward alteration of iron sulfide grains is topotactic where the original iron sulfide microtextures and crystal morphologies are mostly preserved (Figures 2d–2i, 3b-3e). The smaller unit cell of magnetite in comparison to greigite (Chang, Rainford, et al., 2009; Chang et al., 2008; Skinner et al., 1964), and the distinctly different crystal structure of pyrrhotite can explain the polycrystallinity of the neoformed magnetite and pyrrhotite (Figures 3m–3p).

5. A New Multi-Phase Self-Reversed Chemical Remanence Magnetization Mechanism Involving Greigite Alteration

The co-occurrence of greigite alteration, magnetic softening, and multipolarity NRM behavior suggests that the antiparallel remanence components in these greigite-bearing samples are caused by greigite alteration to magnetite and pyrrhotite. Here we propose a new self-reversal explanation for the antiparallel remanence in diagenetic greigite, where a surface-grown chemical remanent magnetization (CRM) is acquired in the opposite direction to the primary remanence residing in the parent greigite core (Figures 3u–3x). Stoichiometric greigite acquires a near-primary CRM with a single-polarity (Figure 3u). As alteration proceeds, expanded magnetite/pyrrhotite

Figure 2. Backscattered electron (BSE) images (a–i) and energy dispersive spectra (EDS) mapping (j–l) of microtextures in S-type samples PAP-204 (a–b) and PAP-390 (c), (d–f) a T-type sample PAP-301, and (g–i) an M-type sample PAP-441. (j–l) EDS mapping of Fe, O, and S distributions in the sample area (i). Distortion in the upper part of (j–l) is caused by instrumental drift. (m–o) Statistics of single-point EDS data from an M-type sample PAP-441. All presented data are based on EDS atom percentages. The grain size is the diameter of the measured grains obtained from BSE images using the software ImageJ (Schneider et al., 2012). (m) Fe/S ratio equals 0.5 for sulfide grains above ~0.5 μm, indicating a chemical composition of pyrite (FeS_2). For grains below ~0.5 μm, the sulfur content decreases, leading to an increased Fe/S ratio. (n) All except one measured iron sulfide grains contain at least 10% oxygen, and the oxygen content steadily increases for grains with sizes below ~1.5 μm. (o) The Fe/(S + O) ratios are mostly around a hematite-like and magnetite-like cation-to-anion matching. Blue dots and numbers indicate the EDS data points in Figure S6 of the Supporting Information S1. Pyrite: Py.

10.1029/2023GL103885

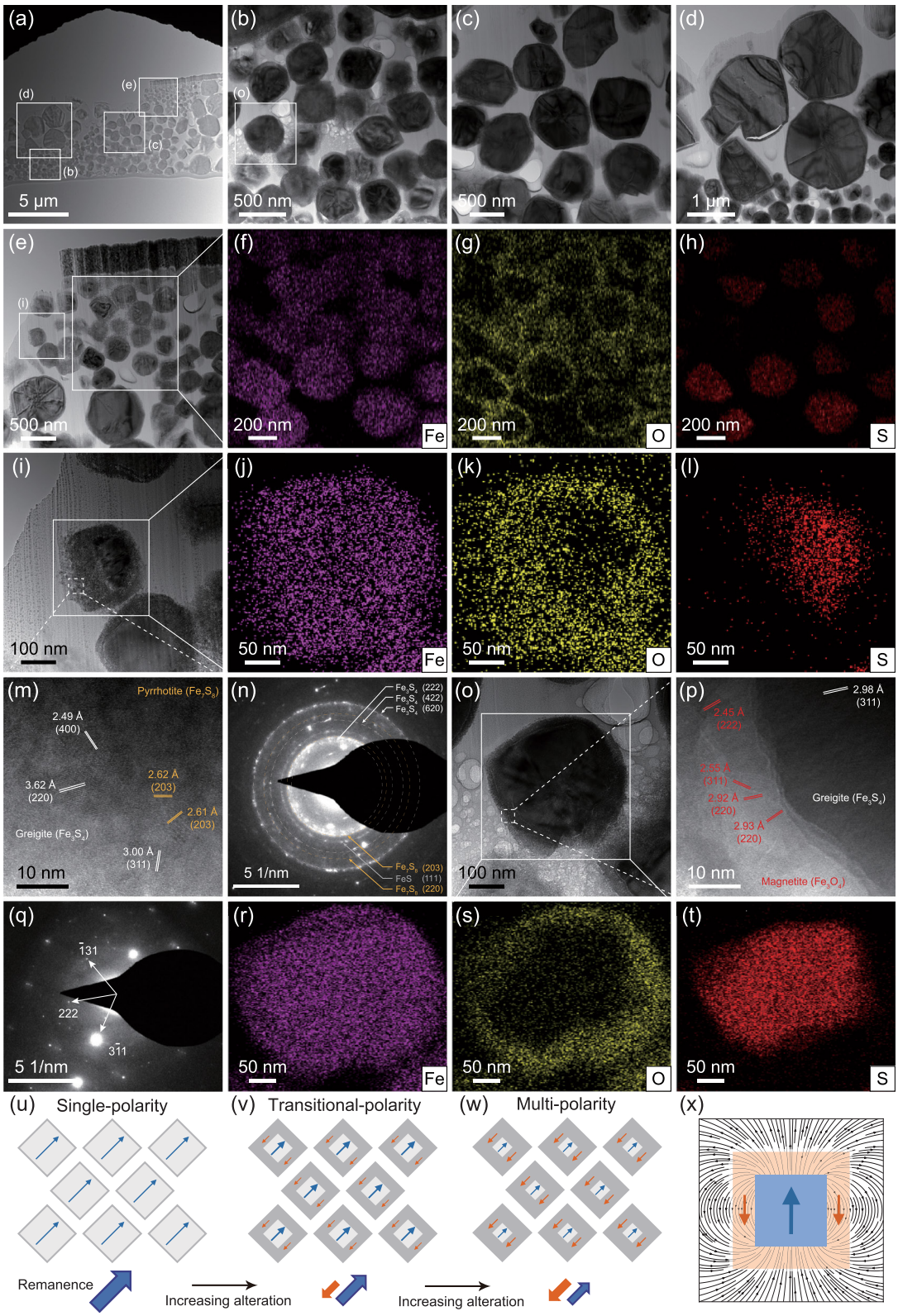

Figure 3.

shells result in a stable self-reversed magnetization (Figures 3v and 3w) as explained next. Surface oxidation/alteration of greigite crystals provides an atomic contact interface between two ferrimagnetic phases: the greigite core and the magnetite/pyrrhotite shell. Ferrimagnetic phases across the phase boundary in partially altered greigite are coupled through an antiparallel remanence ordering (Figures 3v and 3w). The proportion of such self-reversed remanence component to the total remanence would increase as greigite alteration proceeds. But we suspect that this self-reversing component would not grow to a completion, because at some stage the decreasing magnetic energy of the greigite core would not be large enough to overcome the magnetic energy needed to magnetize the newly formed magnetic shell, resulting in a multipolarity remanence. Kelder et al. (2018) showed that the self-reversed component in some samples is stronger than the initial magnetization, but it is not known when the self-reversal magnetization process stops as alteration proceeds.

Néel (1951) originally proposed two classes of self-reversal models for thermoremanent magnetization (TRM): single-phase and multi-phase. The single-phase self-reversal model was used to explain the acquisition of antiparallel remanence in titanomagnetites with high Ti substitutions and high oxidation states during cooling of igneous rocks (Doubrovine & Tarduno, 2004; Verhoogen, 1956). Cation substitution (i.e., Ni) was reported for natural greigite (Chang et al., 2014; Van Velzen et al., 1993). SEM- and TEM-based EDS analyses, however, did not reveal detectable cation substitutions in the studied iron sulfides and their oxidized counterparts. There is also currently no known N-type ferrimagnetic behavior, where the saturation magnetization—the net sublattice magnetization—changes sign in comparison to the stoichiometric phase for any oxidized phases of magnetite or greigite. So, the single-phase model of Néel (1951) is less likely to explain the suggested self-reversal for greigite, where significant cation substitution in greigite would be required.

The antiparallel components of remanence behavior in the greigite-bearing samples studied here can be better explained using the multi-phase self-reversal model of Néel (1951). The multi-phase model deals with TRMs and involves two (or more) interacting ferro- or ferrimagnetic phases with different blocking temperatures during cooling. First, the high-blocking temperature phase acquires a TRM in the direction of the external geomagnetic field. The low-blocking temperature phase then acquires a TRM that is antiparallel to the TRM direction of the high-blocking temperature phase, through antiparallel coupling facilitated either by magnetostatic interaction or exchange interaction that produces much stronger local fields than the external magnetic field (Figure 3x). Here, we extend this multi-phase self-reversal model for TRMs to CRMs, where the late formation of a magnetically softer magnetite/pyrrhotite shell on the surface of the magnetically harder greigite core can in principle acquire a self-reversed CRM component of the shell. Acquisition of this self-reversed CRM is analogous to the self-reversed TRM of the lower blocking-temperature phase with respect to an earlier TRM of the higher blocking phase during cooling of igneous rocks (Dunlop & Özdemir, 1997; Krása et al., 2005). Our model also shares similarities to the core-shell "nanophase" self-reversal model for the ilmenite-hematite solid solution (Prévot et al., 2001). Micromagnetic simulation indicates that magnetostatic interaction coupling of two-layered magnetic phases is able to produce a self-reversed TRM of the oxidized shell (Krása et al., 2005). We suspect that magnetostatic interaction between the shell magnetic phase and the magnetic core in altered greigite is more likely to explain the self-reversal CRM acquisition (Figure 3x).

6. Geochronological, Tectonic, and Paleoenvironmental Implications

The alteration mechanism with different oxidation/alteration degree of greigite could explain the observed anomalous paleomagnetic remanence with variable polarity components of opposite direction in greigite-bearing sediments (Figures 1 and 3u–3x). The low-(un)blocking temperature and high-(un)blocking temperature components were interpreted to be a quasi syn-depositional remanent magnetization carried by early diagenetic greigite (Kelder et al., 2018). For the medium-(un)blocking temperature remanence component, unlike the interpretation of remagnetization due to late greigite growth in silicate sheets by Kelder et al. (2018), we here interpret this opposite remanence component is a self-reversed magnetization acquired during surface alteration of greigite into ferrimagnetic magnetite

Figure 3. (a–t) Transmission electron microscopic (TEM) analyses for a "multi-polarity" sample PAP-441, and (u–x) proposed self-reversal mechanism during progressive greigite alteration. (a) Overview of the focused ion beam (FIB) milled sample and (b–e) mineral aggregates with various grain sizes. Pink (f, j, r), yellow (g, k, s), and red (h, l, t) dots indicate the distribution of the elements Fe, O, and S. White, orange, and red Miller indices (*hkl*) and arrows in (m, n, p, q) indicate greigite, 4C monoclinic pyrrhotite, and magnetite, respectively. Schematic illustration of the self-reversal mechanism: (u) stoichiometric diagenetic greigite without alteration, (v) acquisition of a small portion of self-reversed magnetization of the surface magnetic phases (red-orange arrows) with respect to the more primary chemical remanent magnetization (CRM) carried by the parent greigite core (blue arrows), (w) acquisition of a large self-reversed CRM component with extensive alteration, (x) acquisition of a self-reversal CRM in a partially altered greigite crystal facilitated by the magnetostatic interaction field of the greigite core that exceeds the external fields, and/or the strong exchange interactions across the alteration interface.

and pyrrhotite. The medium-temperature remanence component with a typical demagnetization range of 230°–250°C to 300°–310°C is broadly consistent with the unblocking temperature for monoclinic pyrrhotite with a Curie temperature (T_C) of 320°C and nanophase magnetite with reduced blocking temperature compared to the 580°C T_C of bulk magnetite. This could explain why the later-acquired, self-reversed component often resides in the middle part of the blocking temperature spectrum that is lower than the blocking temperature of early diagenetic greigite.

Alteration of greigite and pyrite in the sedimentary environments may be related to percolation of oxic fluids in different geological settings (e.g., Huang et al., 2017; Rowan & Roberts, 2006) to produce magnetite, or at specific temperature, pH and redox conditions, to produce pyrrhotite (e.g., Dinarès-Turell & Dekkers, 1999; Larrasoaña et al., 2007). Thus, specific post-depositional sedimentary conditions can cause remagnetization and multipolarity remanence in diagenetic greigite. The self-reversal mechanism as argued for here, provides a radically new view on the cause and timing of remanence acquisition in greigite-bearing sediments, which is critical for correct interpretations of paleomagnetic signals from greigite-bearing sedimentary strata for geochronological, tectonic and paleoenvironmental implications.

The self-reversal mechanism is suggested to explain some paleomagnetic records of igneous rocks (Doubrovine & Tarduno, 2004; Dunlop & Özdemir, 1997; Krása et al., 2005; Prévot et al., 2001; Swanson-Hysell et al., 2011), but it is very rarely reported in sedimentary records. Sedimentary examples include possible self-reversal in Arctic sediments due to seafloor oxidation of titanomagnetite (Channell & Xuan, 2009), and self-reversed CRM carried by Al-substituted hematite in red soils (Liu et al., 2022). Recognition of self-reversed remanence in greigite had so far not been proven but is important for paleomagnetic interpretations. We therefore suggest that the antiparallel remanence in greigite-bearing sediments from thermal demagnetization, particularly with a small heating step in the 230–310°C temperature range, should be investigated for a possible self-reversal. With the typical 30°C or larger temperature steps in the 200–350°C range, the self-reversed component may have been overlooked in some previous paleomagnetic studies on greigite-bearing sediments. Possible diagnostics of self-reversal in greigite include: (a) antiparallel remanence component in the demagnetization temperature range of 230°–250°C to 300°–310°C, (b) magnetic softening with reduced coercivity, M_{rs}/M_s, SIRM/κ values, and absence of GRM behavior compared to typical SD diagenetic greigite, (c) grain surface alteration of greigite into pyrrhotite/magnetite under TEM/SEM observations.

7. Conclusions

The present study investigates the origin of the antiparallel NRM components in greigite-bearing sediments from the Pannonian Basin (Hungary), and a novel case of self-reversed magnetization is proposed to explain the long-standing enigma of anomalous remanence carried by greigite. Integrated paleomagnetic, rock magnetic, and electron microscopic analyses indicate that the "multi-polarity" samples with opposite NRM components contain abundant altered iron sulfides, mostly with polycrystalline magnetite and pyrrhotite shells in contact with greigite cores, whereas the "single-polarity" samples contain nearly stoichiometric greigite and pyrite without significant alteration. The alteration (i.e., oxidation and pyrrhotization) is topotactic, and the oxidation extent of the iron sulfides is grain-size dependent, with higher oxidation degree for smaller greigite and pyrite grains because of their larger surface area to volume ratio.

A new self-reversal model is proposed to explain the observed multipolarity magnetization in greigite-bearing sediments, where the surficial magnetite or pyrrhotite acquired a later CRM that is coupled in the opposite direction with the (quasi-)primary remanence of the greigite core. The antiparallel remanence coupling in the alteration interface is more likely facilitated through magnetostatic interaction (and less likely through exchange interaction). That is, the local magnetic field in the shell region produced by the greigite core is much stronger than the external geomagnetic field. This multi-phase self-reversal model is directly supported by TEM-based chemical mapping and electron diffraction analyses. Future work, including nanoscale magnetic imaging and micromagnetic simulation will help to assess and validate this proposed grain-growth self-reversal model.

Recognition of a self-reversal mechanism in greigite-bearing sediments has profound implications for understanding the long-standing problem of their anomalous remanence behavior. Realization of the environmental cause and timing of the antiparallel remanence acquisition is important for a correct interpretation of paleomagnetic records from greigite-bearing sediment sequences that are widely used for geochronology, tectonics, and paleoenvironmental reconstructions.

Data Availability Statement

Paleomagnetic and rock magnetic data, magnetic parameters, and fitted coercivity of remanence component parameters, and energy dispersive spectra data for the studied samples can be downloaded from the Zenodo repository (https://doi.org/10.5281/zenodo.7925726).

Acknowledgments
The authors acknowledge Electron Microscopy Laboratory of Peking University for the use of Helios G4 UX FIB and FEI Tecnai F20 TEM, and Jun Xu and Xiumei Ma for technical assistance. We thank Nick Kelder for measuring the thermal demagnetization data, Rong Huang for measuring some of the low-temperature MPMS data, Andrew Roberts for providing instrumental access to the VSM at the ANU, and Pengxiang Hu and Xiang Zhao for assistance in measurements. We are grateful to editor Monika Korte for efficient handling of this paper, Gillian Turner, and an anonymous reviewer for providing constructive comments. This study was financially supported by the National Natural Science Foundation of China (Grants 41974074, 42061130214, 41722402), and a Royal Society-Newton Advanced Fellowship (NAF\R1\201096) to L.C.

References

Bai, F., Chang, L., Pei, Z., Harrison, R. J., & Winklhofer, M. (2022). Magnetic biosignatures of magnetosomal greigite from micromagnetic calculation. *Geophysical Research Letters*, *49*(10), e2022GL098437. https://doi.org/10.1029/2022GL098437

Bai, F., Chang, L., Xue, P., & Wang, S. (2022). Decomposing isothermal remanent curves and development of a batch processing tool BatchUnMix. *Chinese Journal of Geophysics*, *65*(12), 4789–4801.

Berner, R. A. (1984). Sedimentary pyrite formation: An update. *Geochimica et Cosmochimica Acta*, *48*(4), 605–615. https://doi.org/10.1016/0016-7037(84)90089-9

Chang, L., Rainford, B. D., Stewart, J. R., Ritter, C., Roberts, A. P., Tang, Y., & Chen, Q. (2009). Magnetic structure of greigite (Fe_3S_4) probed by neutron powder diffraction and polarized neutron diffraction. *Journal of Geophysical Research*, *114*(B7), B07101. https://doi.org/10.1029/2008JB006260

Chang, L., Roberts, A. P., Rowan, C. J., Tang, Y., Pruner, P., Chen, Q., & Horng, C. S. (2009). Low-temperature magnetic properties of greigite (Fe_3S_4). *Geochemistry, Geophysics, Geosystems*, *10*(1), Q01Y04. https://doi.org/10.1029/2008GC002276

Chang, L., Roberts, A. P., Tang, Y., Rainford, B. D., Muxworthy, A. R., & Chen, Q. (2008). Fundamental magnetic parameters from pure synthetic greigite (Fe_3S_4). *Journal of Geophysical Research*, *113*(B6), B06104. https://doi.org/10.1029/2007JB005502

Chang, L., Vasiliev, I., van Baak, C., Krijgsman, W., Dekkers, M. J., Roberts, A. P., et al. (2014). Identification and environmental interpretation of diagenetic and biogenic greigite in sediments: A lesson from the Messinian Black Sea. *Geochemistry, Geophysics, Geosystems*, *15*(9), 3612–3627. https://doi.org/10.1002/2013GC005162

Channell, J. E. T., & Xuan, C. (2009). Self-reversal and apparent magnetic excursions in Arctic sediments. *Earth and Planetary Science Letters*, *284*(1–2), 124–131. https://doi.org/10.1016/j.epsl.2009.04.020

Chen, A. P., Berounsky, V. M., Chan, M. K., Blackford, M. G., Cady, C., Moskowitz, B. M., et al. (2014). Magnetic properties of uncultivated magnetotactic bacteria and their contribution to a stratified estuary iron cycle. *Nature Communications*, *5*(1), 4797. https://doi.org/10.1038/ncomms5797

Day, R., Fuller, M., & Schmidt, V. A. (1977). Magnetic hysteresis properties of synthetic titanomagnetites. *Physics of the Earth and Planetary Interiors*, *13*(4), 260–267. https://doi.org/10.1016/0031-9201(77)90108-X

Dinarès-Turell, J., & Dekkers, M. J. (1999). Diagenesis and remanence acquisition in the lower Pliocene Trubi marls at Punta di Maiata (southern Sicily): Palaeomagnetic and rock magnetic observations. In D. H. Tarling & P. Turner (Eds.), *Palaeomagnetism and diagenesis in sediments* (Vol. 151, pp. 53–69). Geological Society, London, Special Publications.

Doubrovine, P. V., & Tarduno, J. A. (2004). Self-reversed magnetization carried by titanomaghemite in oceanic basalts. *Earth and Planetary Science Letters*, *222*(3–4), 959–969. https://doi.org/10.1016/j.epsl.2004.04.009

Dunlop, D. J. (2002). Theory and application of the day plot (M_{rs}/M_s versus H_{cr}/H_c): 1. Theoretical curves and tests using titanomagnetite data. *Journal of Geophysical Research*, *107*(B3), 2056. https://doi.org/10.1029/2001JB000486

Dunlop, D. J., & Özdemir, Ö. (1997). *Rock magnetism: Fundamentals and frontiers* (p. 573). Cambridge University Press.

Farina, M., Esquivel, D. M. S., & Lins de Barros, H. G. P. (1990). Magnetic iron-sulphur crystals from a magnetotactic microorganism. *Nature*, *343*(6255), 256–258. https://doi.org/10.1038/343256a0

Florindo, F., & Sagnotti, L. (1995). Palaeomagnetism and rock magnetism at the upper Pliocene Valle Ricca (Rome, Italy) section. *Geophysical Journal International*, *123*(2), 340–354. https://doi.org/10.1111/j.1365-246X.1995.tb06858.x

Fu, Y., von Dobeneck, T., Franke, C., Heslop, D., & Kasten, S. (2008). Rock magnetic identification and geochemical process models of greigite formation in Quaternary marine sediments from the Gulf of Mexico (IODP Hole U1319A). *Earth and Planetary Science Letters*, *275*(3–4), 233–245. https://doi.org/10.1016/j.epsl.2008.07.034

Harrison, R. J., & Feinberg, J. M. (2008). FORCinel: An improved algorithm for calculating first-order reversal curve distributions using locally weighted regression smoothing. *Geochemistry, Geophysics, Geosystems*, *9*(5), Q05016. https://doi.org/10.1029/2008GC001987

Horng, C. S., Torii, M., Shea, K. S., & Kao, S. J. (1998). Inconsistent magnetic polarities between greigite- and pyrrhotite/magnetite-bearing marine sediments from the Tsailiao-chi section, southwestern Taiwan. *Earth and Planetary Science Letters*, *164*(3–4), 467–481. https://doi.org/10.1016/S0012-821X(98)00239-8

Huang, W., Lippert, P. C., Dekkers, M. J., Jackson, M. J., Zhang, Y., Li, J., et al. (2017). Remagnetization of the Paleogene Tibetan Himalayan carbonate rocks in the Gamba area: Implications for reconstructing the lower plate in the India-Asia collision. *Journal of Geophysical Research: Solid Earth*, *122*(2), 808–825. https://doi.org/10.1002/2016JB013662

Kelder, N. A., Sant, K., Dekkers, M. J., Magyar, I., van Dijk, G. A., Lathouwers, Y. Z., et al. (2018). Paleomagnetism in Lake Pannon: Problems, pitfalls, and progress in using iron sulfides for magnetostratigraphy. *Geochemistry, Geophysics, Geosystems*, *19*(9), 3405–3429. https://doi.org/10.1029/2018GC007673

Krása, D., Shcherbakov, V. P., Kunzmann, T., & Petersen, N. (2005). Self-reversal of remanent magnetization in basalts due to partially oxidized titanomagnetites. *Geophysical Journal International*, *162*(1), 115–136. https://doi.org/10.1111/j.1365-246x.2005.02656.x

Kruiver, P. P., Dekkers, M. J., & Heslop, D. (2001). Quantification of magnetic coercivity components by the analysis of acquisition curves of isothermal remanent magnetization. *Earth and Planetary Science Letters*, *189*(3–4), 269–276. https://doi.org/10.1016/S0012-821X(01)00367-3

Larrasoaña, J. C., Roberts, A. P., Musgrave, R. J., Gràcia, E., Piñero, E., Vega, M., & Martínez-Ruiz, F. (2007). Diagenetic formation of greigite and pyrrhotite in marine sedimentary systems containing gas hydrates. *Earth and Planetary Science Letters*, *261*(3–4), 350–366. https://doi.org/10.1016/j.epsl.2007.06.032

Liu, C., Qin, H., Ferré, E. C., Wang, W., He, K., & Deng, C. (2022). Importance of hematite self-reversal in Al-rich soils magnetostratigraphy: Revisiting the Damei red soil sequence in the Bose Basin, Southern China. *Journal of Geophysical Research: Solid Earth*, *127*(4), e2021JB023165. https://doi.org/10.1029/2021jb023165

Liu, J., Shi, X., Liu, Q., Ge, S., Liu, Y., Yao, Z., et al. (2014). Magnetostratigraphy of a greigite-bearing core from the South Yellow Sea: Implications for remagnetization and sedimentation. *Journal of Geophysical Research: Solid Earth*, *119*(10), 7425–7441. https://doi.org/10.1002/2014JB011206

Lurcock, P. C., & Wilson, G. S. (2012). PuffinPlot: A versatile, user-friendly program for paleomagnetic analysis. *Geochemistry, Geophysics, Geosystems*, *13*(6), Q06Z45. https://doi.org/10.1029/2012GC004098

Magyar, I., Sztanó, O., Sebe, K., Katona, L., Csoma, V., Görög, Á., et al. (2019). Towards a high-resolution chronostratigraphy and geochronology for the Pannonian stage: Significance of the Paks cores (central Pannonian Basin). *Földtani Közlöny*, *149*(4), 351–370. https://doi.org/10.23928/foldt.kozl.2019.149.4.351

Mann, S., Sparks, N. H. C., Frankel, R. B., Bazylinski, D. A., & Jannasch, H. W. (1990). Biomineralization of ferrimagnetic greigite (Fe_3S_4) and iron pyrite (FeS_2) in a magnetotactic bacterium. *Nature*, *343*(6255), 258–261. https://doi.org/10.1038/343258a0

Morin, F. J. (1950). Magnetic susceptibility of αFe_2O_3 and αFe_2O_3 with added titanium. *Physical Review*, *78*(6), 819–820. https://doi.org/10.1103/PhysRev.78.819.2

Néel, L. (1951). L'inversion de l'animantation permanente des roches. *Annales de Géophysique*, *7*, 90–102.

Néel, L. (1955). Some theoretical aspects of rock-magnetism. *Advances in Physics*, *4*(14), 191–243. https://doi.org/10.1080/00018735500101204

Özdemir, Ö., Dunlop, D. J., & Moskowitz, B. M. (1993). The effect of oxidation on the Verwey transition in magnetite. *Geophysical Research Letters*, *20*(16), 1671–1674. https://doi.org/10.1029/93gl01483

Prévot, M., Hoffman, K. A., Goguitchaichvili, A., Doukhan, J. C., Shcherbakov, V., & Bina, M. (2001). The mechanism of self-reversal of thermoremanence in natural hemoilmenite crystals: New experimental data and model. *Physics of the Earth and Planetary Interiors*, *126*(1–2), 75–92. https://doi.org/10.1016/s0031-9201(01)00245-x

Reinholdsson, M., Snowball, I., Zillen, L., Lenz, C., & Conley, D. J. (2013). Magnetic enhancement of Baltic Sea sapropels by greigite magnetofossils. *Earth and Planetary Science Letters*, *366*, 137–150. https://doi.org/10.1016/j.epsl.2013.01.029

Roberts, A. P., Chang, L., Rowan, C. J., Horng, C. S., & Florindo, F. (2011). Magnetic properties of sedimentary greigite (Fe_3S_4): An update. *Reviews of Geophysics*, *49*(1), RG1002. https://doi.org/10.1029/2010RG000336

Roberts, A. P., Pike, C. R., & Verosub, K. L. (2000). First-order reversal curve diagrams: A new tool for characterizing the magnetic properties of natural samples. *Journal of Geophysical Research*, *105*(B12), 28461–28475. https://doi.org/10.1029/2000JB900326

Roberts, A. P., & Weaver, R. (2005). Multiple mechanisms of remagnetization involving sedimentary greigite (Fe_3S_4). *Earth and Planetary Science Letters*, *231*(3–4), 263–277. https://doi.org/10.1016/j.epsl.2004.11.024

Rochette, P., Fillion, G., Mattéi, J.-L., & Dekkers, M. J. (1990). Magnetic transition at 30–34 Kelvin in pyrrhotite: Insight into a widespread occurrence of this mineral in rocks. *Earth and Planetary Science Letters*, *98*(3–4), 319–328. https://doi.org/10.1016/0012-821X(90)90034-U

Rowan, C. J., & Roberts, A. P. (2005). Tectonic and geochronological implications of variably timed remagnetizations carried by authigenic greigite in fine-grained sediments from New Zealand. *Geology*, *33*(7), 553–556. https://doi.org/10.1130/G21382.1

Rowan, C. J., & Roberts, A. P. (2006). Magnetite dissolution, diachronous greigite formation, and secondary magnetizations from pyrite oxidation: Unravelling complex magnetizations in Neogene marine sediments from New Zealand. *Earth and Planetary Science Letters*, *241*(1–2), 119–137. https://doi.org/10.1016/j.epsl.2005.10.017

Sagnotti, L., Roberts, A. P., Weaver, R., Verosub, K. L., Florindo, F., Pike, C. R., et al. (2005). Apparent magnetic polarity reversals due to remagnetization resulting from late diagenetic growth of greigite from siderite. *Geophysical Journal International*, *160*(1), 89–100. https://doi.org/10.1111/j.1365-246X.2005.02485.x

Schneider, C. A., Rasband, W. S., & Eliceiri, K. W. (2012). NIH image to ImageJ: 25 years of image analysis. *Nature Methods*, *9*(7), 671–675. https://doi.org/10.1038/nmeth.2089

Skinner, B. J., Erd, R. C., & Grimaldi, F. S. (1964). Greigite, the thio-spinel of iron: A new mineral. *American Mineralogist*, *49*, 543–555.

Snowball, I. F. (1997). Gyroremanent magnetization and the magnetic properties of greigite-bearing clays in southern Sweden. *Geophysical Journal International*, *129*(3), 624–636. https://doi.org/10.1111/j.1365-246X.1997.tb04498.x

Swanson-Hysell, N. L., Feinberg, J. M., Berquó, T. S., & Maloof, A. C. (2011). Self-reversed magnetization held by martite in basalt flows from the 1.1-billion-year-old Keweenawan rift, Canada. *Earth and Planetary Science Letters*, *305*(1-2), 171–184. https://doi.org/10.1016/j.epsl.2011.02.053

Tauxe, L., Bertram, H. N., & Seberino, C. (2002). Physical interpretation of hysteresis loops: Micromagnetic modeling of fine particle magnetite. *Geochemistry, Geophysics, Geosystems*, *3*(10), 1055–1122. https://doi.org/10.1029/2001GC000241

Turner, G. M. (2001). Toward an understanding of the multicomponent magnetization of uplifted marine sediments in New Zealand. *Journal of Geophysical Research*, *106*(B4), 6385–6397. https://doi.org/10.1029/2000JB900406

Van Velzen, A. J., Dekkers, M. J., & Zijderveld, J. D. A. (1993). Magnetic iron-nickel sulfides in the Pliocene and Pleistocene marine marls from the Vrica section (Calabria, Italy). *Earth and Planetary Science Letters*, *115*(1–4), 43–55. https://doi.org/10.1016/0012-821x(93)90211-q

Vasiliev, I., Franke, C., Meeldijk, J. D., Dekkers, M. J., Langereis, C. G., & Krijgsman, W. (2008). Putative greigite magnetofossils from the Pliocene Epoch. *Nature Geoscience*, *1*(11), 782–786. https://doi.org/10.1038/ngeo335

Verhoogen, J. (1956). Ionic ordering and self-reversal in impure magnetites. *Journal of Geophysical Research*, *61*(2), 201–209. https://doi.org/10.1029/jz061i002p00201

Wang, S., & Chang, L. (2022). Rock magnetic signatures of hydrothermal mineralization in the Trans-Atlantic Geotraverse (TAG) hydrothermal field. *Geochemistry, Geophysics, Geosystems*, *23*(5), e2022GC010368. https://doi.org/10.1029/2022GC010368

References From the Supporting Information

Zhou, W., Peacor, D. R., Van der Voo, R., & Mansfield, J. F. (1999). Determination of lattice parameter, oxidation state, and composition of individual titanomagnetite/titanomaghemite grains by transmission electron microscopy. *Journal of Geophysical Research*, *104*(B8), 17689–17702. https://doi.org/10.1029/1999jb900095